Journal Name

ARTICLE TYPE

Geometry and Mechanics of Thin Growing Bilayers[†]

Matteo Pezzulla,[a] Gabriel P. Smith,[a] Paola Nardinocchi,[b] and Douglas P. Holmes[*a]

We investigate how thin sheets of arbitrary shapes morph under the isotropic in-plane expansion of their top surface, which may represent several stimuli such as nonuniform heating, local swelling and differential growth. Inspired by geometry, an analytical model is presented that rationalizes how the shape of the disk influences morphing, from the initial spherical bending to the final isometric limit. We introduce a new measure of slenderness that describes a sheet in terms of both thickness and plate shape. We find that the mean curvature of the isometric state is three fourth's the natural curvature, which we verify by numerics and experiments. We finally investigate the emergence of a preferred direction of bending in the isometric state, guided by numerical analyses. The scalability of our model suggests that it is suitable to describe the morphing of sheets spanning several orders of magnitude.

Cylindrically curved thin structures result from the nano-scale fabrication of semiconductor nanotubes[1–4], and the nonuniform heating[5], local swelling[6], and differential growth[7] of thin sheets. For laminated composites[8], electrolytic thin film deposition[9,10], and concrete slabs[11], this cylindrical curling presents an engineering challenge, while recent work has utilized it as a mechanism for stimuli responsive self-assembly[12,13]. The length scales of these examples range from the nanometer to the meter, suggesting that geometry dominates the deformation processes. Mechanically, these structures are bilayer disks in which one layer expands relative to the other either isotropically or not[14]. In this paper, we show that in the asymptotic limit of large bilayer growth, any arbitrarily shaped disk will adopt a cylindrical shape whose mean curvature is three-fourth's the natural curvature. We present an analytical model that captures both the bifurcation from spherical to cylindrical curvature [*] and the isometric limit, verified by numerics and experiments.

1 Geometry and Mechanics

Let us consider a thin body subjected to a dome-like (elliptic) natural curvature – this may be thought of as the result of swelling, growth, or heating of the top surface. Within the context of non-Euclidean plates[15], the body may be modeled as a shell having
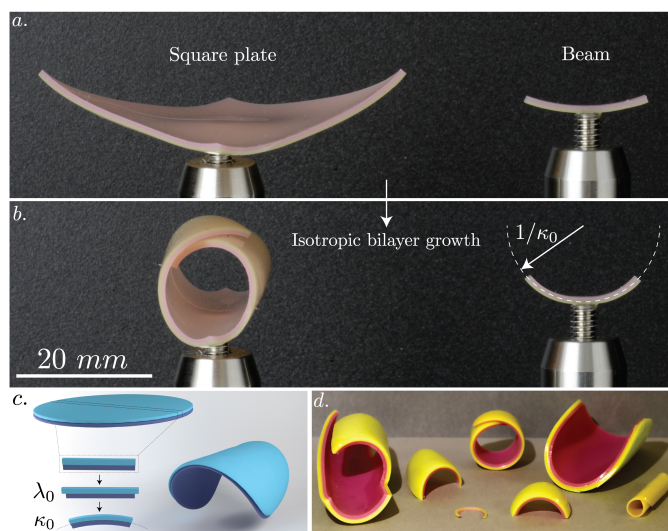
Fig. 1 (a) A bilayer disk and the beam cut from it. (b) Isometric limit. (c) Measuring the natural curvature of the disk as the realized curvature of the beam. (d) Isometric states obtained by residual swelling of disks having different shapes.

the following first and second natural fundamental forms

$$\bar{\mathbf{a}} = \Lambda_o^2 \begin{pmatrix} 1 & 0 \\ 0 & 1 \end{pmatrix}, \quad \bar{\mathbf{b}} = \kappa_o \begin{pmatrix} 1 & 0 \\ 0 & 1 \end{pmatrix}. \tag{1}$$

The natural stretch Λ_o and natural curvature κ_o represent the lateral distances and curvatures that would make the sheet locally stress-free. However, as every surface in space must fulfill the Gauss-Codazzi-Mainardi equations, it is not usually possible for the sheet to realize the natural forms. Conversely, if a beam is cut

[a] Department of Mechanical Engineering, Boston University, Boston, MA, 02215; E–mail: dpholmes@bu.edu
[b] Sapienza Università di Roma, via Eudossiana 18, Roma, Italy.
[*] For simple geometries, *e.g.* circles and ellipses, this shape evolution can be described semi-analytically by making an assumption about either the potential function or displacement field.

from the sheet, its inherent 1D geometry will allow it to adopt a three-dimensional shape with longitudinal axis stretch and curvature equal to Λ_o and κ_o, respectively, without any need of satisfying additional constraints. This strong connection between the sheet and the beam provides a simple means to evaluate the natural forms of the former by measuring the deformed shape of the latter [see figure 1 (c)].

1.1 Theory and experiments

To fully exploit this idea, we fabricated bilayer disks by spincoating the two layers made of polyvinylsiloxane (PVS) Zhermack Elite Double 32 and 8, respectively, as shown in figure 1 (a-b). Free chains flow from the softer (pink) to the stiffer (green) polymer by residual swelling[16], corresponding to a dome-like natural curvature, and a conformal natural stretch. Mechanically, this corresponds to a bilayer disk where the top layer has been stretched homothetically by a factor λ^{-1} and then bound to the bottom layer. This results in a discontinuous three-dimensional natural metric $\bar{\mathbf{g}}$ that may be approximated[17] as $\bar{\mathbf{g}} = \bar{\mathbf{a}} - 2z\bar{\mathbf{b}}$, where z is the coordinate along the thickness. Approximate expressions for $\bar{\mathbf{a}}$ and $\bar{\mathbf{b}}$ as functions of pre-stretches were derived in Ref. 17, albeit the natural curvature was then measured experimentally as the curvature of very small strips cut along principal directions. We overcome the lack of a predictive expression for the natural curvature by imaginarily cutting a beam from the sheet, and determining its deformed shape analytically by following Ref. 18 as $\Lambda_o = \Lambda_o(\lambda, m, n)$ and $\kappa_o = \kappa_o(\lambda, m, n)/h$, where m and n are top-to-bottom thicknesses and Young moduli ratios, respectively, and h is the thickness of the sheet (see Appendix). Therefore, the natural forms are determined analytically as functions of λ and the material and geometrical ratios.

A comparison of the energies for stretching and bending suggests that a sheet exposed to such stimuli should adopt an isometric deformation in the limit of large stretch. We analytically describe the realization of this *asymptotic isometry*, corresponding to a zero Gaussian curvature K and a nearly stretch-free sheet. The dimensionless energy of the shell may be written as[17]

$$\overline{\mathscr{U}} = \int \left[(1-\nu)|\mathbf{a} - \bar{\mathbf{a}}|^2 + \nu \mathrm{tr}^2(\mathbf{a} - \bar{\mathbf{a}})\right]\sqrt{|\bar{\mathbf{a}}|}dA + \tag{2}$$
$$+ \frac{h^2}{3}\int \left[(1-\nu)|\mathbf{b} - \bar{\mathbf{b}}|^2 + \nu \mathrm{tr}^2(\mathbf{b} - \bar{\mathbf{b}})\right]\sqrt{|\bar{\mathbf{a}}|}dA\,,$$

where $\mathbf{a}$ and $\mathbf{b}$ are the first and second fundamental forms of the mid-surface of the deformed sheet, respectively. In the *isometric limit*, we have $\mathbf{a} = \bar{\mathbf{a}}$ and the stretching energy is zero. To find the deformation of the disk we then minimize the bending energy under the constraint that the mid-surface be flat, since $\mathbf{a} = \bar{\mathbf{a}} = \Lambda_o^2\mathbf{I}$. We write $\mathbf{b}$ in cartesian coordinates (u,v) so that the second fundamental form is $Ldu^2 + 2Mdudv + Ndv^2$, and impose the constraint of a flat mid-surface by enforcing that its Gaussian curvature $\Lambda_o^{-4}(LN - M^2)$ be zero through a Lagrange multiplier.

2 Isometric limit

For the characterization of the *isometric limit*, we assume that the energy density is homogenous. Consequently, for the total energy
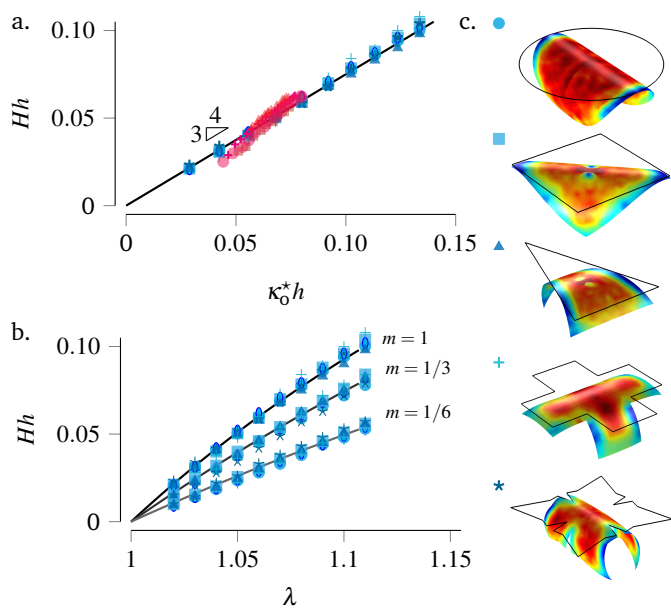
Fig. 2 (a) Dimensionless mean curvature versus dimensionless rescaled natural curvature: the three-fourth law excellently captures numerical and experimental data regardless of initial shape. Numerical data (blue) refers to circle, square, leaf-like, triangle, cross and ellipse, each for different thicknesses, and experimental data (red) refers to a square, cross, triangle, and circle. (b) Dimensionless mean curvature versus λ: the isometric limit is expressed in terms of the stretch of the top layer. Three different master curves are shown, each corresponding to different thicknesses ratios m. (c) Isometric shapes from COMSOL with the color code representing the mean curvature.

to be minimized, it suffices to minimize its density augmented by the constraint on the Gaussian curvature imposed by the Lagrange multiplier. The minimization gives $L + N = \kappa_o(1 + \nu)$ and $K = 0$, a solution solely in terms of the principal invariants of the curvature tensor, and independent of the shape of the sheet: if a homogeneous energy density is assumed, no information on the bending direction can be obtained[19]. The result of the minimization may be rewritten in terms of the mean curvature H of the sheet as $H = \frac{1}{2}a^{\alpha\beta}b_{\alpha\beta} = \frac{1}{2}\bar{a}^{\alpha\beta}b_{\alpha\beta} = \frac{1}{2}\Lambda_o^{-2}(L+N)$. If the material is incompressible ($\nu = 1/2$), it becomes

$$H = \frac{3}{4}\frac{\kappa_o}{\Lambda_o^2}\,, \tag{3}$$

that is, in the limit of large stretch, the mean curvature of the sheet is three-fourth of the rescaled natural curvature $\kappa_o^\star = \kappa_o/\Lambda_o^2$, regardless of the shape of the sheet. Equivalently, the sheet morphs into a cylinder of radius $R = 1/(2H)$. Since $\kappa_o \sim 1/h$ whereas Λ_o does not depend on the thickness, we derive $H \sim 1/h$.

2.1 Experiments and numerics

To verify our analytical prediction, we carried out experiments and numerical simulations. In the experiments, we measured the curvatures of disks of several shapes and the corresponding beams during residual swelling [figure 1 (a-b)] by image analysis performed using Matlab. Numerical simulations were per-

formed to solve the geometrical problem within the context of finite (incompatible) tridimensional elasticity with large distortions using a Neo-Hookean incompressible material model[20] implemented in the commercial software COMSOL Multiphysics. The sheets were made of two layers: as the top one was pre-stretched by λ^{-1}, it was subjected to a distortion field $\mathbf{F}_o = \lambda(\mathbf{e}_1 \otimes \mathbf{e}_1 + \mathbf{e}_2 \otimes \mathbf{e}_2) + \mathbf{e}_3 \otimes \mathbf{e}_3$, whereas the bottom one was not pre-stretched and therefore subjected to $\mathbf{F}_o = \mathbf{I}$. We simulated several shapes and thicknesses, and verified that the mean curvature H was homogeneous apart from boundary layers near the edges. Then we plotted the product Hh as a function of the dimensionless natural curvature $\kappa_o^\star h$, or the stretch λ via the 1D analytical model, in the limit of large stretch. The numerical data referring to different thicknesses and the experimental data collapse to a single master curve thus verifying the analytical prediction that $H \sim 1/h$ and the three-fourth law excellently predicts the mean curvature of the sheet regardless of its shape as shown in figure 2 (a). Figure 2 (b) shows how the dimensionless mean curvature varies with the stretch of the top layer and how it is affected by the thicknesses ratio m, providing a design rule for bilayer sheets; all the data corresponding to different thicknesses and shapes collapses to master curves.

2.2 Energy comparison

To predict and explain the transition that turns a spherical growth into a flat state[19], we start from the energy in equation (2) and compare the energies of the spherical and isometric states, without any *a priori* assumptions of a stress state or displacement. These assumptions usually rely on the consideration of an Airy stress function, which is known only for a very small number of sheet's shapes, and on the account of a linearized version of the Gauss's theorem[10,21–23]. Away from large stretches, the two principal curvatures are equal to each other and homogeneous throughout the sheet. However, the morphing into a spherical cap ($L = N$) becomes too costly for the sheet when the stretch, or the natural curvature, reaches a critical value. While for small values of κ_o, it is convenient for the sheet to stretch and increase its Gaussian curvature, above a critical threshold of κ_o, it is cheaper to morph isometrically. Assuming a metric with constant Gaussian curvature in Gaussian normal coordinates as in 16, the dimensionless stretching energy may be written as $\overline{\mathscr{U}}_s = (1/9)\Lambda_o^6 K^2 \int r^4 dA$, where r is the undeformed radial coordinate, and we define $\mathscr{S} = (2/9 \int r^4 dA/A)^{1/4}$ as the shape factor. Also, as $L = N$, the dimensionless bending energy is $\overline{\mathscr{U}}_b = h^2 \Lambda_o^{-2} A(L - \kappa_o)^2$, where A is the undeformed area of the incompressible sheet. As $K^2 \simeq \Lambda_o^{-8} L^4$ before bifurcation, the total dimensionless energy for the spherical cap is

$$\overline{\mathscr{U}}_{bb} = (1/9)L^4 \Lambda_o^{-2} \int r^4 dA + h^2 A \Lambda_o^{-2}(L - \kappa_o)^2, \quad (4)$$

while the total energy of the isometric shape is equal to

$$\overline{\mathscr{U}}_{ab} = (1/4)h^2 A \Lambda_o^{-2} \kappa_o^2, \quad (5)$$

which becomes smaller than the energy of the spherical cap above a critical value of the natural curvature as figure 3 shows (see
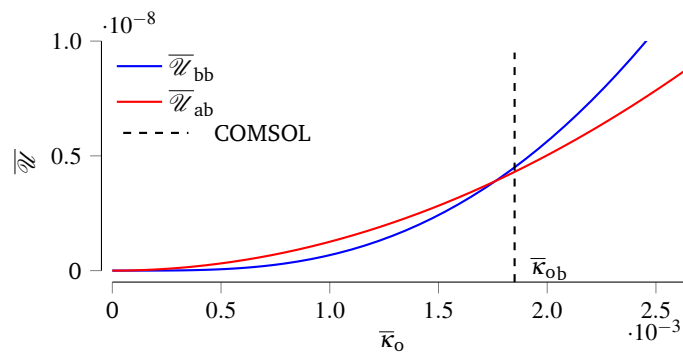
Fig. 3 Dimensionless energies before (blue) and after (red) bifurcation versus the natural curvature. Our model predicts bifurcation as the intersection between the two energies, which is in good agreement with the numerical threshold determined in COMSOL (dashed line).

Appendix for the complete derivation). This analytical reasoning suggests that a bifurcation between the two principal curvatures must occur at a critical κ_{ob} to drive the sheet into an isometric shape.

2.3 Pre-bifurcation curvature

As our model does not rely on any *a priori* assumption on the stress state or displacements, it is suitable to study the pre-bifurcation morphing of the sheets, regardless of their shapes. Minimization of the total energy $\overline{\mathscr{U}}_{bb}$ with respect to L yields

$$\overline{L}^3 + \gamma^4(\overline{L} - \overline{\kappa}_o) = 0, \quad (6)$$

where curvatures have been nondimensionalized by $1/h$ and denoted with bars. The geometrical dimensionless small parameter $\gamma = h/\mathscr{S}$ encloses the shape of the sheet in the equilibrium equation and may be computed easily by its definition. The smaller γ is, the more slender the structure is in terms of both thickness and plate shape. Equation (6) can be solved analytically and it admits just one real solution $L(\kappa_o)$ or, equivalently via the 1D model, $L(\lambda)$.
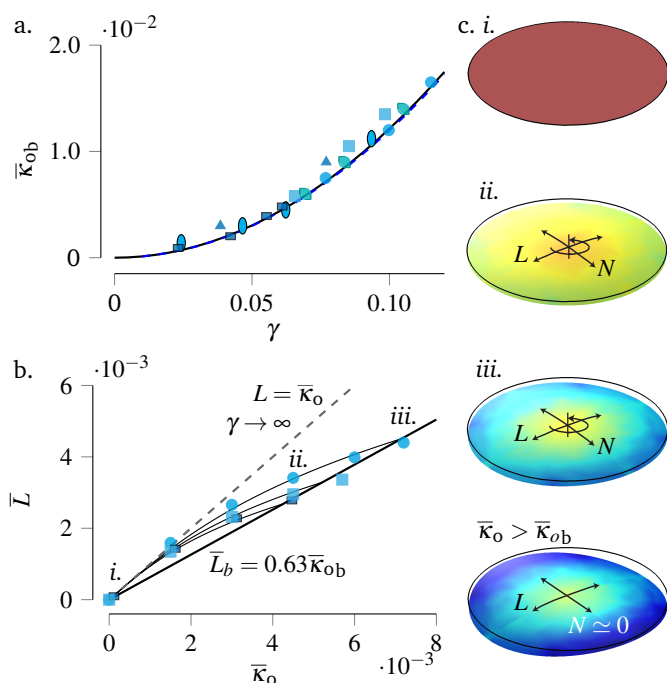
2.4 Bifurcation curvature

When the natural curvature reaches a value such that the energy of the spherical cap coincides with the energy of the isometric state, bifurcation occurs; the equality between the two energies may be written as

$$\frac{1}{2}\overline{L}_b^4 + \gamma^4\left(\overline{L}_b^2 - 2\overline{L}_b\overline{\kappa}_{ob} + \frac{3}{4}\overline{\kappa}_{ob}^2\right) = 0, \quad (7)$$

where the subscript b denotes quantities at bifurcation. This is a perturbation problem in the smallness parameter γ that multiplies the bending factor of equation (7). Seeking a perturbation expansion solution in the form $L_b = L_{b0} + \gamma^4 L_{b1} + O(\gamma^8)$, we obtain $L_b \simeq \kappa_{ob}/2$, at the leading order. Moreover, by Taylor expanding equation (7) in γ up to $O(\gamma^{31/3})$, we derive a shape-dependent formula for the bifurcation natural curvature

$$\overline{\kappa}_{ob} = \sqrt{\frac{20 + 14\sqrt{2}}{27}}\gamma^2. \quad (8)$$

Fig. 4 (a) Dimensionless natural curvature at bifurcation versus γ: the analytical prediction given by (8) (solid line), in agreement with the numerical solution (dashed) of (7), perfectly predicts the finite element simulation results (symbols) obtained for different shapes (identified by the shape of the symbol) and thicknesses. (b) Pre-bifurcation behavior in terms of $\bar{L}(\bar{\kappa}_o)$ for different shapes (circle, square, rectangle) obtained by finite element simulations (symbols) and analytics (solid lines). The two straight lines identify the upper and lower bounds corresponding to a bending-dominated solution and the bifurcation point, respectively. (c) Deformed shapes of a thin circular disk from COMSOL.

Differently from other works in the literature, this formula remarkably predicts the natural curvature at bifurcation for thin sheets having different shapes. While curvatures scale as $1/h$ as we showed, this formula predicts that the bifurcation natural curvature scales as h. The analytical solution $L(\kappa_o)$, evaluated at bifurcation through equation (8), yields $L_b = 0.63\kappa_{ob}$, an analytical relation that does not depend on γ, and refines our previous asymptotic estimate. Figure 4 (a) shows the dimensionless natural curvature at bifurcation for different geometries (different γ): the analytical model excellently predicts the threshold for different shapes and thicknesses that have been simulated in COMSOL provided that the shape is convex. The dashed blue curve corresponds to the numerical solution of equation (7), which justifies the asymptotic analysis that led to equation (8). The model is also capable of distinguishing the pre-bifurcation behavior that sheets of different convex shapes exhibit as figure 4 (b) shows. For clarity, we reported the pre-bifurcation solution for three shapes. As $\gamma \to \infty$, bending dominates stretching and equation (6) yields $\bar{L} = \bar{\kappa}_o$. This is also an upper-bound for all the shapes as $\bar{L}' = \gamma^4/(\gamma^4 + 3\bar{L}^2)$ that is maximum at $\bar{\kappa}_o = 0$ where it is equal to 1 regardless of the shape: the realized curvature never exceeds the natural curvature. Also, we plotted the relation between realized and natural curvatures at bifurcation, which sets a lower-bound

for $\bar{L}$. Figure 4 (c) shows the numerical deformed shape of a circular disk as the stretch increases: the disk morphs from a flat state to a spherical cap before bifurcating into a cylinder. The analytical model is not capable of describing the spherical bending and the bifurcation of concave shapes, whose topological defects presumably affect their behavior[24]. Notably, the three-fourth law holds regardless of the shape, whether convex or concave.

3 Bending direction

Finally, we investigate the emergence of a preferred direction of bending following bifurcation by running several simulations with different meshes. While it was shown that the principal curvatures of an ellipse have no preferred orientation[19], here we show that nearly all shapes select a particular direction for their generators immediately after symmetry is broken. Cylindrical generators orient themselves along an axis which preserves reflection symmetry. If multiple planes of reflection symmetry exist for a particular shape, bending will occur along the longest length of the disk (Fig. 5a). For instance, a square of length a and width b has two unique planes of reflection symmetry, and has been observed to bend along its diagonal[25]. We show with a series of simulations for $a = 0.02$ m and $h = 0.4$ mm that as a/b is increased, and the disk transitions from square to rectangular, the orientation of the generators transitions from the diagonal to the short length b. Curiously, this transition does not occur immediately once $a/b > 1$, as a logistic analysis of the orientation data identifies a transition at $a/b = 1.028 \pm 0.0025$. A preferred bending direction in rectangular sheets has been attributed to boundary layers effects[26] that lower the energy in the disk[27]. Our results help generalize these findings for any arbitrary shape. The notion of a preferred bending direction upon bifurcation does not contradict Mansfield's classical results, as the cylindrical generators can be rotated to any arbitrary angle while remaining in equilibrium when perturbed via mechanical or chemical stimuli[6].
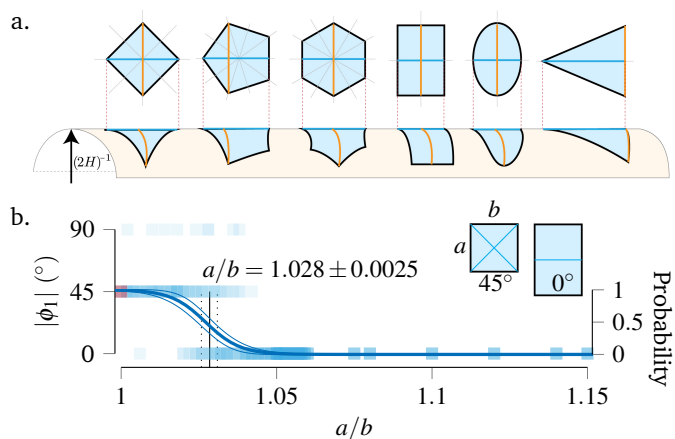
Fig. 5 (a) Numerical statistics of preferred generators (blue) for different shapes. (b) Logistic analysis of the orientation data of the transition from a square to a rectangle.

4 Conclusions

In summary, we have derived a theoretical analytical model that describes the morphing of disks subjected to dome-like natural curvatures, regardless of their shape. We also showed the emergence of an isometric limit with analytics, numerics and experiments, underlying the importance of isometries in mechanics[28]. The capability to morph 2D shapes into 3D shells by in-plane[16] and transverse residual swelling opens intriguing avenues towards the precise design of soft structures.

Acknowledgements

A Natural axis stretch and curvature

For the sake of clarity, we explicitly write the expressions for Λ_o and κ_o derived in 18:

$$\Lambda_o = \frac{\lambda \left[\lambda + mn(3 + \lambda + m(3 + m + m^2 n + 3(1+m)\lambda))\right]}{m^4 n^2 + 2m(2 + m(3+2m))n\lambda + \lambda^2}, \quad (9)$$

$$\kappa_o = -\frac{6}{h}\frac{(\lambda-1)m(1+m)^2 n(m^4 n^2 + 2m(2+m(3+2m))n\lambda + \lambda^2)}{\lambda\left[\lambda + mn(3+\lambda + m(3+m+m^2 n + 3(1+m)\lambda))\right]^2}. \quad (10)$$

B Derivation of the energies away from the isometric limit

In response to isotropic bilayer growth, a thin sheet will deform into a spherical cap for low degrees of stretching. Therefore, its two principal curvatures are equal and the metric must be axially symmetric. In polar coordinates, $\bar{\mathbf{a}}$ may be expressed as

$$\bar{\mathbf{a}} = \Lambda_o^2 \begin{pmatrix} 1 & 0 \\ 0 & r^2 \end{pmatrix}.$$

Also, curvatures may be approximated as homogeneous throughout the sheet so that the Gaussian curvature is constant and positive. As we did in Ref. 16, we look for metrics with constant Gaussian curvature in Gaussian normal coordinates (ρ, θ) where the first fundamental form may be expressed as $ds^2 = d\rho^2 + a_{\theta\theta}d\theta^2$ and

$$a_{\theta\theta} = \left(\frac{1}{\sqrt{K}}\sin\sqrt{K}\rho\right)^2 = \rho^2 - \frac{K}{3}\rho^4 + O(\rho^5),$$

where we also Taylor expanded the metric around $\rho = 0$. We recall that $\rho(r) = \int_0^r \sqrt{a_{rr}(r')}dr'$, where a_{rr} is the radial component of the metric. Notice that, before bifurcation, curvatures are small and the Taylor approximation can be applied. Finally, symmetry yields $a_{r\theta} = \bar{a}_{r\theta} = 0$ and we approximate, as in Ref. 16, $a_{rr} \simeq \bar{a}_{rr}$. This approximation yields $\rho(r) = \Lambda_o r$. Finally, the stretching energy may be written as

$$\overline{\mathscr{U}}_s = \int \frac{(a_{\theta\theta} - \Lambda_o^2 r^2)^2}{\Lambda_o^2 r^3}drd\theta = \frac{1}{9}\Lambda_o^6 K^2 \int r^4 dA, \quad (11)$$

where we computed the Gaussian curvature $K = \det\mathbf{b}/\det\mathbf{a}$ as $\Lambda_o^{-4}L^2$. This formula corresponds to $\det\mathbf{b}/\det\bar{\mathbf{a}}$ and should be used just in the isometric state. However, before bifurcation the metric does not diverge much from the natural metric and this expression of the Gaussian curvature is a good approximation. Notably, the stretching energy does not depend on ν.

As the metric does not diverge much from the target metric before bifurcation, the second fundamental form may be expressed as a homogeneous field. Consequently, the (dimensionless) bending energy may be written as

$$\overline{\mathscr{U}}_b = \frac{2}{3}(1+\nu)h^2\Lambda_o^{-2}A(L-\kappa_o)^2, \quad (12)$$

which in the limit $\nu \to 1/2$ coincides with the bending energy presented in the main paper.

After bifurcation, the stretching energy drops to zero as the stretch is increased slightly beyond the bifurcation threshold while the bending energy does not. As the Gaussian curvature in the isometric state is zero, we can take $M = N = 0$ and L such that equation (14) holds, that is $L = (1+\nu)\kappa_o$. The (dimensionless) energy of the isometric states then reads

$$\overline{\mathscr{U}}_{ab} = \frac{h^2}{3}(1-\nu^2)A\Lambda_o^{-2}\kappa_o^2, \quad (13)$$

which in the limit $\nu \to 1/2$ coincides with the energy presented in the main paper.

C Compressible materials

C.1 Isometric limit

When $\mathbf{a} = \bar{\mathbf{a}}$, the total energy is just of the bending type. The functional to be minimized corresponds to the bending energy augmented by a constraint in the form of a Lagrange multiplier, η, placed on the Gaussian curvature to prevent stretching of the mid–plane, it reads

$$f(L,M,N,\eta) = \Lambda_o^{-4}\Big[(1-\nu)[(L-\kappa_o)^2 + 2M^2 + (N-\kappa_o)^2] +$$

$$+ \nu[(L-\kappa_o)^2 + (N-\kappa_o)^2 + 2(L-\kappa_o)(N-\kappa_o)] - \eta(LN-M^2)\Big].$$

Minimization yields

$$\frac{\partial f}{\partial \eta} = 0 \Leftrightarrow LN - M^2 = 0,$$

$$\frac{\partial f}{\partial L} = 0 \Leftrightarrow 2(1-\nu)(L-\kappa_o) + 2\nu(L-\kappa_o) + 2\nu(N-\kappa_o) - \eta N = 0,$$

$$\frac{\partial f}{\partial N} = 0 \Leftrightarrow 2(1-\nu)(N-\kappa_o) + 2\nu(N-\kappa_o) + 2\nu(L-\kappa_o) - \eta L = 0,$$

$$\frac{\partial f}{\partial M} = 0 \Leftrightarrow \eta = -2(1-\nu).$$

This algebraic system yields $K = \Lambda_o^{-4}(LN-M^2) = 0$ and $L+N = (1+\nu)\kappa_o$. The mean curvature of the isometric state may be then written as

$$H = \frac{1}{2}a^{\alpha\beta}b_{\alpha\beta} = \frac{1}{2}\bar{a}^{\alpha\beta}b_{\alpha\beta} = \frac{1}{2}\Lambda_o^{-2}(L+N) = \frac{1+\nu}{2}\frac{\kappa_o}{\Lambda_o^2}, \quad (14)$$

which in the limit $\nu \to 1/2$ coincides with the three–fourth law

(equation (3) in the main paper).

Finally, the rescaled natural curvature $\kappa_o^\star = \kappa_o/\Lambda_o^2$ turns out to be the natural curvature in the rescaled coordinate system $\xi^\alpha = \Lambda_o \eta^\alpha$, where ξ^α and η^α are the new and old curvilinear coordinates, respectively. Indeed, the fundamental forms in the new system are $\bar{\mathbf{a}}^\star = \Lambda_o^{-2}\bar{\mathbf{a}} = \mathbf{I}$ and $\bar{\mathbf{b}}^\star = \Lambda_o^{-2}\bar{\mathbf{b}} = \kappa_o^\star\mathbf{I}$. These coordinate transformation demonstrates that the couple $(\bar{\mathbf{a}},\bar{\mathbf{b}})$ determines a mean curvature in the isometric limit equal to the one determined by $(\bar{\mathbf{a}}/\Lambda_o^2, \bar{\mathbf{b}}/\Lambda_o^2)$, when $\bar{\mathbf{a}}$ is Euclidean.

C.2 Bifurcation

Bifurcation occurs when the energy of the spherical cap becomes equal to the energy of the cylinder, $\overline{\mathscr{U}}_{bb} = \overline{\mathscr{U}}_{ab}$. Enforcing this equality, we get

$$\frac{1}{9}L^4\int r^4 dA + \frac{2}{3}(1+\nu)h^2A(L-\kappa_o)^2 = \frac{h^2}{3}(1-\nu^2)A\kappa_o^2.$$

Recalling the definition of the shape factor $\mathscr{S} = (2/9\int r^4 dA/A)^{1/4}$, $\gamma = h/\mathscr{S}$ and working in dimensionless quantities, we get

$$\frac{1}{2}\bar{L}_b^4 + \frac{1+\nu}{3}\gamma^4\left(2\bar{L}_b^2 - 4\bar{L}_b\bar{\kappa}_{ob} + (1+\nu)\bar{\kappa}_{ob}^2\right) = 0, \qquad (15)$$

which in the limit $\nu \to 1/2$ coincides with equation (5) in the main paper. Notice that the first term comes from the stretching energy whereas the second one, multiplying γ^4, is the difference between bending energies before and after bifurcation.

By Taylor expanding equation (15) in γ up to $O(\gamma^{31/3})$, we derive a shape-dependent formula for the bifurcation natural (dimensionless) curvature $\bar{\kappa}_{ob} = f(\nu)\gamma^2$. The expression of $f(\nu)$ is cumbersome, yet analytical. We report its plot in figure 6 (a). In the limit $\nu \to 1/2$, it coincides with equation (8) in the main paper as $f(1/2) = \sqrt{(20+14\sqrt{2})/27}$. Notice how material and geometry couple in a multiplicative way: the function f depends just on the material while γ depends just on geometry.

Equation (15) represents a perturbation problem in the smallness parameter γ that multiplies the bending factor. Seeking a perturbation expansion solution in the form $L_b = L_{b0} + \gamma^4 L_{b1} + O(\gamma^8)$, we obtain

$$L_b \simeq \left(1 - \sqrt{\frac{1-\nu}{2}}\right)\kappa_{ob}, \qquad (16)$$

at the leading order, which in the limit $\nu \to 1/2$ coincides with the asymptotic estimate given in the paper $L_b \simeq \kappa_{ob}/2$. This result comes from the leading order balance of energies that sets the stretching energy aside, being just a balance of bending contents, before and after the bifurcation. In the main text, when $\nu = 1/2$, we analytically refined this estimate getting $L_b = 0.63\kappa_{ob}$. This scalar pre-factor has been rounded off for simplicity, due to the cumbersome analytical expression

$$L_b = \frac{3^{1/6}(-3^{1/6} + (3\sqrt{2} + \sqrt{18+\sqrt{3}})^{2/3})}{2\sqrt{2}(3\sqrt{2} + \sqrt{18+\sqrt{3}})^{1/3}}\kappa_{ob}.$$

Furthermore, when $\nu \neq 1/2$, we derived $L_b = g(\nu)\kappa_{ob}$ where the
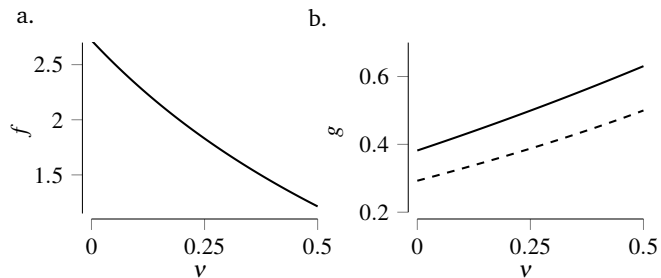
Fig. 6 (a) The function f versus ν. (b) The function g versus ν (solid line) and its asymptotic approximation (dashed line).

function $g(\nu)$ is analytical and depends just on material properties. As the expression of $g(\nu)$ is cumbersome, we report its plot in figure 6 (b) as well as its asymptotic approximation shown in equation (16). Notice that $g(1/2) = 0.63$.

C.3 Pre-bifurcation

To predict the pre-bifurcation morphing of the disk, we have to minimize the total energy of the spherical cap

$$\overline{\mathscr{U}}_{bb} = \frac{1}{9}L^4\Lambda_o^{-2}\int r^4 dA + \frac{2}{3}(1+\nu)h^2\Lambda_o^{-2}A(L-\kappa_o)^2.$$

By working in the dimensionless quantities, minimization yields

$$\bar{L}^3 + \frac{2(1+\nu)}{3}\gamma^4(\bar{L}-\bar{\kappa}_o) = 0, \qquad (17)$$

which in the limit $\nu \to 1/2$ coincides with equation (6) in the main paper. This equation can be solved analytically to get $L(\kappa_o)$ or, equivalently via the 1D model, $L(\lambda)$.

References

1 R. Tenne, L. Margulis, M. Genut and G. Hodes, *Nature*, 1992, **360**, 444–446.

2 O. G. Schmidt, N. Schmarje, C. Deneke, C. Müller and N.-Y. Jin-Phillipp, *Adv. Mater.*, 2001, **13**, 756–759.

3 O. G. Schmidt and K. Eberl, *Nature*, 2001, **410**, 168–168.

4 G. Stoychev, S. Zakharchenko, S. Turcaud, J. W. C. Dunlop and L. Ionov, *ACS Nano*, 2012, **6**, 3925–3934.

5 K. Seffen and R. McMahon, *Int. J. Mech. Sci.*, 2007, **49**, 230 – 238.

6 D. P. Holmes, M. Roché, T. Sinha and H. A. Stone, *Soft Matter*, 2011, **7**, 5188–5193.

7 M. B. Amar and A. Goriely, *J. Mech. Phys. Solids*, 2005, **53**, 2284–2319.

8 M. W. Hyer, *J. Compos. Mater.*, 1981, **15**, 175–194.

9 G. G. Stoney, *P. Roy. Soc. Lond. A Mat.*, 1909, **82**, 172–175.

10 L. Freund, *J. Mech. Phys. Solids*, 2000, **48**, 1159 – 1174.

11 J. M. Armaghani, T. J. Larsen and L. L. Smith, *Temperature response of concrete pavements*, 1987.

12 J.-H. Cho, T. James and D. H. Gracias, *Adv. Mater.*, 2010, **22**, 2320–2324.

13 D. H. Gracias, *Curr. Opin. in Chem. Eng.*, 2013, **2**, 112 – 119.

14 Z. Chen, Q. Guo, C. Majidi, W. Chen, D. J. Srolovitz and M. P. Haataja, *Phys. Rev. Lett.*, 2012, **109**, 114302.

15 E. Efrati, E. Sharon and R. Kupferman, *J. Mech. Phys. Solids*, 2009, **57**, 762 – 775.

16 M. Pezzulla, S. A. Shillig, P. Nardinocchi and D. P. Holmes, *Soft Matter*, 2015, **11**, 5812–5820.

17 S. Armon, E. Efrati, R. Kupferman and E. Sharon, *Science*, 2011, **333**, 1726–1730.

18 A. Lucantonio, P. Nardinocchi and M. Pezzulla, *P. Roy. Soc. Lond. A Mat.*, 2014, **470**, 20140467.

19 E. H. Mansfield, *P. Roy. Soc. Lond. A Mat.*, 1965, **288**, 396–417.

20 A. Lucantonio, P. Nardinocchi, M. Pezzulla and L. Teresi, *Smart Mater. Struct.*, 2014, **23**, 045043.

21 E. H. Mansfield, *The Bending and Stretching of Plates*, Cambridge University Press, 1989.

22 K. Seffen, *P. Roy. Soc. Lond. A Mat.*, 2007, **463**, 67–83.

23 K. A. Seffen and C. Maurini, *Journal of the Mechanics and Physics of Solids*, 2013, **61**, 190 – 204.

24 N. P. Bende, R. C. Hayward and C. D. Santangelo, *Soft Matter*, 2014, **10**, 6382–6386.

25 B. Li, Q. Wang, E. Wang, Z. Jia, Y. Yan, Z. Bian, X. Ren, S. Cai and Y. Huang, *Appl. Phys. Lett.*, 2013, **103**, –.

26 S. Alben, B. Balakrisnan and E. Smela, *Nano Lett.*, 2011, **11**, 2280–2285.

27 Y. C. Fung and W. H. Wittrick, *Q. J. Mech. Appl. Math.*, 1955, **8**, 191–210.

28 M. A. Dias and B. Audoly, *J. Elasticity*, 2015, **119**, 49–66.